Synaptic phosphorylated -synuclein in dementia with Lewy bodies

OXFORD UNIVERSITY PRESS | Brain

Synaptic phosphorylated α-synuclein in dementia with Lewy bodies

Journal:	*Brain*
Manuscript ID	BRAIN-2017-00849.R1
Manuscript Type:	Original Article
Date Submitted by the Author:	n/a
Complete List of Authors:	Colom-Cadena, Martí; Hospital de la Santa Creu i Sant Pau- Biomedical Research Institute Sant Pau- Universitat Autònoma de Barcelona, Memory Unit, Department of Neurology; Centro de Investigación Biomédica en Red de Enfermedades Neurodegenerativas. CIBERNED Pegueroles, Jordi; Hospital de la Santa Creu i Sant Pau- Biomedical Research Institute Sant Pau- Universitat Autònoma de Barcelona, Memory Unit, Department of Neurology; Centro de Investigación Biomédica en Red de Enfermedades Neurodegenerativas. CIBERNED, Herrmann, Abbigail; Centre for Cognitive and Neural Systems, Euan MacDonald Centre, and the Centre for Dementia Prevention, Univeristy of Edinburgh Henstridge, Christopher; Centre for Cognitive and Neural Systems, Euan MacDonald Centre, and the Centre for Dementia Prevention, Univeristy of Edinburgh Muñoz-Llahuna, Laia; Hospital de la Santa Creu i Sant Pau- Biomedical Research Institute Sant Pau- Universitat Autònoma de Barcelona, Memory Unit, Department of Neurology; Centro de Investigación Biomédica en Red de Enfermedades Neurodegenerativas. CIBERNED Querol-Vilaseca, Marta; Hospital de la Santa Creu i Sant Pau- Biomedical Research Institute Sant Pau- Universitat Autònoma de Barcelona, Memory Unit, Department of Neurology; Centro de Investigación Biomédica en Red de Enfermedades Neurodegenerativas. CIBERNED Luque-Cabecerans, Joan; Hospital de la Santa Creu i Sant Pau- Biomedical Research Institute Sant Pau- Universitat Autònoma de Barcelona, Memory Unit, Department of Neurology; Centro de Investigación Biomédica en Red de Enfermedades Neurodegenerativas. CIBERNED Clarimon, Jordi; Hospital de la Santa Creu i Sant Pau- Biomedical Research Institute Sant Pau- Universitat Autònoma de Barcelona, Memory Unit, Department of Neurology; Centro de Investigación Biomédica en Red de Enfermedades Neurodegenerativas. CIBERNED Belbin, Olivia; Hospital de la Santa Creu i Sant Pau- Biomedical Research Institute Sant Pau- Universitat Autònoma de Barcelona, Memory Unit, Department of Neurology; Centro de Investigación Biomédica en Red de Enfermedades Neurodegenerativas. CIBERNED Núñez-Llaves, Raúl; Hospital de la Santa Creu i Sant Pau- Biomedical Research Institute Sant Pau- Universitat Autònoma de Barcelona, Memory Unit, Department of Neurology; Centro de Investigación Biomédica en Red de Enfermedades Neurodegenerativas. CIBERNED

	Blesa, Rafael; Hospital de la Santa Creu i Sant Pau- Biomedical Research Institute Sant Pau- Universitat Autònoma de Barcelona, Memory Unit, Department of Neurology; Centro de Investigación Biomédica en Red de Enfermedades Neurodegenerativas. CIBERNED Smith, Colin; University of Edinburgh, Centre for Clinical Brain Sciences McKenzie, Chris-Anne; University of Edinburgh, Centre for Clinical Brain Sciences Frosch, Matthew; Massachusetts General Hospital and Harvard Medical School Roe, Allyson; Massachusetts General Hospital and Harvard Medical School Fortea, Juan; Hospital de la Santa Creu i Sant Pau- Biomedical Research Institute Sant Pau-Universitat Autònoma de Barcelona, Barcelona, Spain.; Centro de Investigación Biomédica en Red de Enfermedades Neurodegenerativas. CIBERNED Andilla, Jordi; ICFO-Institut de Ciències Fotòniques, The Barcelona Institute of Science and Technology, Castelldefels, Barcelona Loza-Alvarez, Pablo; ICFO-Institut de Ciències Fotòniques, The Barcelona Institute of Science and Technology, Castelldefels, Barcelona Gelpi, Ellen; Neurological Tissue Bank of the Biobanc-Hospital Clinic-IDIBAPS Hyman, Bradley; Massachusetts General Hospital and Harvard Medical School Spires-Jones, Tara; Centre for Cognitive and Neural Systems, Euan MacDonald Centre, and the Centre for Dementia Prevention, Univeristy of Edinburgh Lleo, Alberto; Hospital de la Santa Creu i Sant Pau- Biomedical Research Institute Sant Pau- Universitat Autònoma de Barcelona, Memory Unit, Department of Neurology; Centro de Investigación Biomédica en Red de Enfermedades Neurodegenerativas. CIBERNED
Subject category:	Neurodegeneration – cellular and molecular
To search keyword list, use whole or part words followed by an *:	Neuropathology < DEMENTIA, alpha-Synuclein < NEURODEGENERATION: CELLULAR AND MOLECULAR, Axon degeneration < NEURODEGENERATION: CELLULAR AND MOLECULAR, Lewy bodies < NEURODEGENERATION: CELLULAR AND MOLECULAR, Protein aggregation < NEURODEGENERATION: CELLULAR AND MOLECULAR, Synaptopathy < NEURODEGENERATION: CELLULAR AND MOLECULAR

Synaptic phosphorylated α-synuclein in dementia with Lewy bodies

Martí Colom-Cadena[1], Jordi Pegueroles[1], Abigail G. Herrmann[2], Christopher M. Henstridge[2], Laia Muñoz[1], Marta Querol-Vilaseca[1], Carla San Martin[1], Joan Luque-Cabecerans[1], Jordi Clarimon[1], Olivia Belbin[1], Raúl Núñez-Llaves[1], Rafael Blesa[1], Colin Smith[4], Chris-Anne McKenzie[4], Matthew P. Frosch[5], Allyson Roe[5], Juan Fortea[1], Jordi Andilla[6], Pablo Loza-Alvarez[6], Ellen Gelpi[3], Bradley T. Hyman[5], Tara L. Spires-Jones[2*], Alberto Lleó[1*]

[1] Memory Unit, Department of Neurology, Institut d'Investigacions Biomèdiques Sant Pau - Hospital de Sant Pau, Universitat Autònoma de Barcelona, CIBERNED, Barcelona, Spain.

[2] Centre for Cognitive and Neural Systems, Euan MacDonald Centre, and the Centre for Dementia Prevention, University of Edinburgh, Edinburgh, EH8 9JZ, UK.

[3] Neurological Tissue Bank of the Biobanc-Hospital Clinic-IDIBAPS, Barcelona Spain.

[4] University of Edinburgh, Centre for Clinical Brain Sciences, Edinburgh, UK.

[5] Massachusetts General Hospital and Harvard Medical School, Charlestown, MA, USA.

[6]ICFO-Institut de Ciències Fotòniques, The Barcelona Institute of Science and Technology, Castelldefels, Barcelona, Spain.

*These authors have contributed equally.

Corresponding author:

Dr. Alberto Lleó

Department of Neurology, Hospital de la Santa Creu i Sant Pau

Sant Antoni Maria Claret, 167

08025 Barcelona, Spain

Phone: +34935565986 ; Fax:+34935565602

Email: alleo@santpau.es

Running title:

Synaptic p-α-synuclein in DLB

Abstract

Dementia with Lewy bodies ~~(DLB)~~ is characterized by the accumulation of Lewy bodies ~~(LB)~~ and Lewy neurites ~~(LN)~~ in the central nervous system, both of which are composed mainly of aggregated α-synuclein phosphorylated at serine 129 ~~(p-α-synuclein)~~. Although ~~p~~phosphorylated ~~-~~α-synuclein is believed to exert toxic effects at the synapse in DLB and other α-synucleinopathies, direct evidence for the precise synaptic localization has been difficult to achieve due to the lack of adequate optical microscopic resolution to study human synapses. In the present study we applied array tomography, a microscopy technique that combines ultrathin sectioning of tissue with immunofluorescence allowing precise identification of small structures, to quantitatively investigate the synaptic p-α-synuclein pathology in dementia with Lewy bodies~~DLB~~.

We performed array tomography on human brain samples from ~~the cingulate cortex of~~ 5 dementia with Lewy bodies~~DLB~~ patients, 5 Alzheimer's disease patients and 5 healthy controls to analyse the presence of phosphorylated~~p-~~ α-synuclein immunoreactivity at the synapse and their relationship with synapse size. Main analyses were performed in blocks from cingulate cortex and confirmed in blocks from the striatum of DLB cases. A total of 1318700 single pre- or post-synaptic terminals were analysed.

We found that p-α-synuclein is present exclusively in dementia with Lewy bodies~~DLB~~ cases, where it can be identified in the form of Lewy bodies, Lewy neurites ~~LN~~ and small aggregates (<0.16 μm^3). 19-25% of phosphorylated~~p-~~ α-synuclein deposits were found in pre-synaptic terminals mainly in the form of small aggregates. Synaptic terminals that co-localized with small aggregates of phosphorylated~~p-~~ α-synuclein were significantly larger than those that did not. Finally, a gradient of phosphorylated~~p-~~ α-synuclein aggregation in synapses (pre>pre+post>post-synaptic) was observed.

These results indicate that phosphorylatedp- α-synuclein is found at the pre-synaptic terminals of dementia with Lewy bodiesDLB cases mainly in the form of small phosphorylatedp- α-synuclein aggregates that are associated with changes in synaptic morphology. Overall, our data support the notion that pathological phosphorylatedp- α-synuclein may disrupt the structure and function of the synapse in dementia with Lewy bodiesDLB.

Keywords: P-α-synuclein, Dementia with Lewy bodies, Synapses, Array Tomography, Human tissue.

Abbreviations: DLB, dementia with Lewy bodies; LB, Lewy bodies; LN, Lewy neurites; p-α-synuclein, α-synuclein phosphorylated at serine 129; PSD-95, post-synaptic density protein 95.

Introduction

Dementia with Lewy bodies (DLB) is the second most common neurodegenerative dementia after Alzheimer's disease ~~(AD)~~. The neuropathological hallmark of DLB is the formation of spherical inclusions in the neuronal somata called Lewy bodies ~~(LB)~~ and of elongated structures in dendritic or axonal compartments called Lewy neurites ~~(LN)~~ in the central and peripheral nervous systems (Goedert *et al.*, 2013).

In DLB, Lewy bodies~~LBs~~ and Lewy neurites~~LNs~~ are mainly composed of filaments of misfolded α-synuclein protein (Walker *et al.*, 2015). α-synuclein is a synaptic protein that is located in pre-synaptic terminals where it contributes to neurotransmission and synaptic homeostasis (Maroteaux *et al.*, 1988; Iwai *et al.*, 1995; Clayton and George, 1999; Lashuel *et al.*, 2013; Burré, 2015; Calo *et al.*, 2016). Under pathological conditions α-synuclein is phosphorylated at residue serine 129 (p-α-synuclein). This phenomenon occurs constitutively at very low levels, but is markedly enhanced during pathological processes in which p-α-synuclein is detected in >90% of α-synuclein aggregates (Fujiwara *et al.*, 2002; Hasegawa *et al.*, 2002; Saito *et al.*, 2003; Anderson *et al.*, 2006; Muntané *et al.*, 2012). Growing evidence indicates that aggregation of α-synuclein at synapses is a major event in the pathogenesis of DLB and other α-synucleinopathies (Calo *et al.*, 2016). In particular, data from transgenic animal models suggest a toxic role of α-synuclein in synapses (Garcia-Reitböck *et al.*, 2010; Nemani *et al.*, 2010; Lundblad *et al.*, 2012; Calo *et al.*, 2016). In postmortem brains from patients with DLB, p-α-synuclein is detected in synaptic-enriched fractions (Muntané *et al.*, 2008; Walker *et al.*, 2013) and α-synuclein forms small proteinase-k-resistant aggregates in pre-synaptic terminals (Kramer and Schulz-Schaeffer, 2007; Tanji *et al.*, 2010). These data suggest that, although Lewy bodies ~~B~~ and Lewy neurites~~N~~ are the classical hallmarks of DLB and other α-synucleinopathies, accumulation of pathological

α-synuclein at the synapse may be the main effector of the disease leading to synaptic dysfunction and loss. Nonetheless, the study of α-synuclein-mediated synaptic pathology in humans has remained elusive, in part because synapses are small structures difficult to resolve microscopically in human brain.

In the present work we applied array tomography, a technique based on the production of 70nm consecutive sections combined with immunofluorescence, to image synaptic pathology in DLB under the diffraction limit of light (Micheva and Smith, 2007; Kay *et al.*, 2013). Array tomography requires special fixation conditions, which limits the samples available for this type of studies. This technique has been applied previously to successfully demonstrate synaptic abnormalities in animal models of Alzheimer's disease ~~D~~ and in human Alzheimer's disease~~D~~ brains (Koffie *et al.*, 2009, 2012; Jackson *et al.*, 2016). To our knowledge, this study is the first to use array tomography to quantitatively assess synaptic p-α-synuclein in DLB, which allowed us to resolve α-synuclein pathology in synaptic terminals in human brain samples.

Materials and methods

Standard protocol approvals, and patient consents. All brain donors and/or next of kin had given written informed consent for the use of brain tissue for research. The study was approved by the local ethics committee of: the Hospital de Sant Pau, Barcelona, Spain; the Edinburgh Brain Bank ethics committee and the ACCORD medical research ethics committee (approval numbers LR/11/ES/0022, 16/ES/0084, and 15-HV-016; ACCORD is the Academic and Clinical Central Office for Research and Development, a joint office of the University of Edinburgh and NHS Lothian); and the Massachusetts Alzheimer's Disease Research Centre and Massachusetts General Hospital Neuropathology department with local Institutional Review Board regulations.

Subjects. Human brain samples were obtained from the Edinburgh Brain Bank -see **Supplementary Table 1** for Medical Research Council codes-, the Massachusetts Alzheimer's Disease Research Centre and the Neurological Tissue Bank (NTB) of the Biobanc-Hospital Clinic-IDIBAPS in Barcelona.

Brain sampling and processing protocols for neuropathological diagnoses were carried out following international recommendations as previously described (Colom-Cadena *et al.*, 2013; Kay *et al.*, 2013; Samarasekera *et al.*, 2013).

~~Fifteen p~~Patients fulfilling clinical and neuropathological criteria for DLB (n=5) (McKeith *et al.*, 2005), Alzheimer's disease~~D~~ (n=5) (Montine *et al.*, 2012), or healthy control cases (n=5) were included in this study. Clinical and neuropathological data were retrospectively obtained from the clinical charts available at the Edinburgh Brain Bank, the Massachusetts Alzheimer's Disease Research Centre and the NTB. Neuropathological stages were applied according to international recommendations for DLB (McKeith *et al.*, 2005) and~~,~~ Lewy body~~B~~ pathology (Braak *et al.*, 2003). In cases

with concomitant Alzheimer's diseaseD pathology, current National Institute of Ageing/Alzheimer Association guidelines were applied (Montine et al. 2012).

Tissue processing for array tomography. Fresh brain tissue from all cases was processed immediately upon collection for array tomography as previously described (Micheva and Smith, 2007; Kay *et al.*, 2013). The processing was the same for all cases regardless of the collection centre. Briefly, 1mm x 1mm x 3mm tissue blocks from the cingulate cortex comprising all cortical layers and the striatum (nucleus putamen) were sectioned. Tissue blocks were fixed in 4% paraformaldehyde and 2.5% sucrose in 20mM phosphate buffered saline pH 7.4 (PBS) for up to 3 hours. Samples were dehydrated through ascending concentrations of ethanol, embedded into LR White acrylic resin (Electron Microscopy SciencesEMS) and introduced into gelatine capsules where resin was allowed to polymerize overnight at >50ºC. After polymerization, tissue blocks were stored at room temperatureRT until used.

70nm-array production. LR white embedded tissue blocks were cut at 70nm sections using an ultramicrotome (Leica) equipped with an Ultra Jumbo Diamond Knife 35º (Diatome). Ribbons of at least 30 consecutive sections were produced and collected in gelatine subbed coverslips. For each case, two adjacent blocks of the cingulate cortex were processed as described below (see **Fig. 1** for study design).

Immunofluorescence. Coverslips with 70nm consecutive sections were stained as previously described (Kay *et al.*, 2013). Sections were incubated with Tris-Glycine solution 5' at room temperatureRT followed by a blocking of unspecific antigens with a cold water fish blocking buffer (Sigma-Aldrich) for 30 min. Sections were then

incubated for 2 hours with the following primary antibodies: mouse anti-α-synuclein phosphorylated at serine 129 (dilution 1:50, clone P-α-synuclein #64, WAKO), goat anti-synaptophysin (dilution 1:50, AF5555, R&D Systems) and rabbit anti- post-synaptic density protein 95 (-PSD-95) (dilution 1:50, clone D27E11, Cell Signaling), rabbit anti synapsin I (dilution 1:50, AB1543P, Millipore) or rabbit anti--α-synuclein (dilution 1:50, AB5038, Millipore). After Tris buffered salineTBS washings, secondary fluorescent antibodies Alexa 488, Alexa 555 and Alexa 647 (dilution 1:50, Invitrogen) were applied for 30'. Sections were washed with Tris buffered salineTBS and samples were stained with Hoechst 33258 (dilution 1:100, Life Technologies) for 5 min for nuclei visualization. Finally, coverslips were mounted on microscope slides with Immu-Mount (Fisher Scientific) mounting media.

Image acquisition. Images of the same region were acquired in consecutive sections using an Olympus BX61 microscope equipped with: 454, 488, 555 and 647 single-band pass filters (49000, 49002, 49004 and 49009 respectively, Chroma); an Orca Flash 4.0 LT camera (Hamamatsu); and a 64x 1.2NA Plan Apochromat objective (Olympus) controlled with HCImage software (Hamamatsu). For Stimulated Emission Depletion microscopy, images from one representative DLB case were acquired using a TCS 5 Stimulated Emission Depletion CW microscope (Leica Microsystems). The CW Stimulated Emission Depletion laser operates at the wavelength of 592 nm and imaging is performed using hybrid detectors. The system performance has been fully characterized and a complete analysis of the achieved transversal resolution can be found elsewhere (Merino *et al.*, 2017). Sections with omission of antibodies or with secondary antibodies only were imaged to ensure specific and independent fluorophore visualization. For co-localization purposes, images were acquired avoiding saturated

pixels. Saturation was only minimally applied for figure visualization. For each case, three fields of each section were imaged comprising all cortical layers (see **Fig. 1** for details).

Image processing and analysis. Image stacks of each channel comprising all 70nm consecutive sections were first registered as previously described (Kay *et al.*, 2013b) using *Multistackreg 1.4* ImageJ plugin (courtesy of Brad Busse based on (Thévenaz *et al.*, 1998), based on a rigid registration followed by an affine registration of a reference channel that is applied to the other channels.

After alignment, identification of immunofluorescent objects and quantification of overlapping objects was achieved using an in-house semi-automatic algorithm (see **Fig. 1** for details). Aligned sections were segmented using an automated local thresholding. Additionally, objects that were not in at least two consecutive sections were considered background and removed. Segmentation parameters were exclusive for each channel, but were the same for all included cases. A total of 1318700~~1023248~~ single pre- or post-synaptic terminals were identified.

After identification of three-dimensional objects, three different analyses were performed: 1) the density of objects for each channel subtracting the area occupied by cell bodies and/or blood vessels using a mask of the maximum intensity projection of the synaptophysin channel; 2) the proportion of channel objects that overlap with objects from another channel; and 3) the median size of all objects and of those co-localizing (see **Fig. 1** for details). The in-house semi-automatic algorithm can be freely accessed at https://github.com/MemoryUnitSantPau.

Experimental design. The immunostaining, image acquisition, and image processing and analyses were carried out blinded to the clinicopathological diagnosis by assigning a random code to each sample.

Statistical analysis. Kruskal-Wallis with uncorrected Dunn's analysis post-hoc tests were used to compare differences between three groups in p-α-synuclein densities, co-localization percentages or object sizes. Statistical significance was set at 5% ($\alpha = 0.05$). All data were analysed using the Statistical Package for the Social Sciences version 19.0 (SPSS Inc., Chicago, IL, USA).

Results

Demographic, clinical and neuropathologic characteristics of cases

Demographic, clinical and neuropathologic data are shown in **Table 1**. As expected, the DLB group exhibited advanced α-synuclein pathology as assessed by McKeith types and Lewy bodyB Braak stages. A group of healthy subjects and Alzheimer's diseaseD cases were included as controls for the ~~AT~~ array tomography analyses.

P-α-synuclein is located in DLB pre-synaptic terminals

P-α-synuclein immunoreactivity in DLB was detected in array tomography in the form of Lewy bodiesB, Lewy neuritesN as well as small aggregates, the latter being defined as objects <0.16µm^3 without a clear dendritic or axonal morphology (**Fig. 2A-B**). Occasionally, p-α-synuclein immunoreactivity in cell nuclei was also observed. Quantification of total p-α-synuclein aggregates confirmed that pathology was restricted to DLB in ~~this area~~ array tomography, with negligible levels in Alzheimer's diseaseD and controls (**Fig. 2C**). In contrast, immunofluorescence for non-phosphorylated α-synuclein showed a diffuse punctate pattern in grey matter in both controls and DLB. There was a high degree of overlap between p-α-synuclein and non-phosphorylated α-synuclein in DLB aggregates (**Supplementary Fig. 1).** Therefore we chose p-α-synuclein as a marker to investigate the synaptic pathology in DLB.

We found that 19.17±4.4% of p-α-synuclein aggregates co-localized with synaptophysin-positive terminals in the cingulate cortex (**Fig. 2D**, **Supplementary Fig. ~~1~~2**, **Supplementary Mov. 1**). These data were consistent across cases and revealed that most of the p-α-synuclein present at the pre-synapse consisted of small aggregates (76.6±4%), while medium-sized aggregates or Lewy neuritesN were less abundant (23.4±4%). As expected, no co-localization was found between Lewy bodiesB and

synaptic terminals. Of the total synaptophysin-positive synaptic terminals analysed in DLB cases (n= 252696), 2.7±1% contained p-α-synuclein.

The pre-synaptic localization of p-α-synuclein aggregates was confirmed using synapsin I as an additional pre-synaptic marker. We found that 25.9±7.3% of p-α-synuclein aggregates co-localized with synapsin I-positive terminals (**Supplementary Fig. 3**). As expected, most synapsin I-positive terminals co-localized with synaptophysin.

We used the striatum (putamen) as an additional region to confirm these findings. We found that 19.68±12.7% of p-α-synuclein aggregates in the putamen were co-localizing with synaptophysin-positive pre-synaptic terminals.

Pre-synaptic terminal size and p-α-synuclein aggregation

Synaptic terminals that co-localized with small aggregates of p-α-synuclein were 1.43±0.17-fold larger than those that did not (p=0.014, **Fig. 3**). Interestingly, this difference was not observed when comparing the size of synaptophysin terminals without p-α-synuclein with those that co-localized with LNs.

Trans-synaptic localization of p-α-synuclein

Trans-synaptic propagation of p-α-synuclein pathology has been proposed as a common mechanism in synucleinopathies (Recasens and Dehay, 2014). To investigate this phenomenon *in vivo*, we next selected those synaptophysin pre-synaptic terminals that were opposed to objects labelled with the post-synaptic terminal marker PSD-95 (**Fig. 4A**). In those paired terminals we observed that p-α-synuclein was more frequently located in pre-synaptic terminals (49.82±4.3%, **Fig. 4B**), followed by a both pre- and post-synaptic localization (33.99±2.4%) and less frequently in the post-synaptic density

only (16.18±3%). The synaptic gradient of p-α-synuclein was also observed in the striatum, with a more pronounced pre-synaptic predominance (70.14±11.2% pre-synaptic-only, 23.13±13.7% pre- and post-synaptic, 6.73±5.2% post-synaptic only). The post-synaptic terminal localization of p-α-synuclein was also confirmed by using Stimulated Emission Depletion microscopy in order to increase the lateral resolution (**Fig. 4C**). These data confirm that although p-α-synuclein aggregates are preferentially located at the pre-synapse, they can be independently found at the post-synapse as well.

Discussion

In the present study we have shown by array tomography that aggregates of p-α-synuclein were present at the synapse in DLB cases. In pre-synaptic terminals, the majority of p-α-synuclein was found in the form of small aggregates, while other types of aggregates, like Lewy bodies~~B~~ or Lewy neurites~~N~~, are less abundant. Moreover, these small aggregates were associated with structural changes in pre-synaptic terminals. Finally, we observed a gradient of p-α-synuclein aggregates from the pre- to post-synaptic compartments.

There is growing evidence that synaptic abnormalities in DLB precede neuronal loss and Lewy bodies~~B~~ formation (Chung *et al.*, 2009; Nikolaus *et al.*, 2009; Calo *et al.*, 2016; Henstridge *et al.*, 2016) and that these synaptic defects ~~may be~~are closely related with clinical symptoms (Vallortigara *et al.*, 2014; Whitfield *et al.*, 2014; Bereczki *et al.*, 2016). However, the investigation of DLB as a primary synaptopathy has been hampered by our technical ability to study synapses in human brain. The small size of synaptic terminals falls under the diffraction limit of light, which limits the use of conventional optical microscopy techniques for this purpose. Electron microscopy, which has been the standard technique to resolve the structure of synapses, only permits the reconstruction of small brain volumes and is less amenable to labelling multiple proteins (O'Rourke *et al.*, 2012).

In the present work we applied array tomography to image synaptic pathology in DLB under the diffraction limit of light (Micheva and Smith, 2007; Kay *et al.*, 2013). To our knowledge, this is the first study to apply array tomography in DLB brains, a technique that has allowed us to perform large-scale quantitative synaptic imaging. We analysed 1318700~~1023248~~ single pre- or post-synaptic terminals together with p-α-synuclein with very high spatial resolution. Previous studies have investigated synaptic proteins in

DLB brains using conventional immunohistochemistry (Wakabayashi *et al.*, 1994; Revuelta *et al.*, 2008; Scott *et al.*, 2010) or biochemical analysis of brain homogenates (Masliah *et al.*, 1993; Brown *et al.*, 1998; Hansen *et al.*, 1998; Campbell *et al.*, 2000; Reid *et al.*, 2000; Kramer and Schulz-Schaeffer, 2007; Mukaetova-Ladinska *et al.*, 2013; Khundakar *et al.*, 2016; Xing *et al.*, 2016). In some of these studies, p-α-synuclein and proteinase-k resistant α-synuclein aggregates were found in synaptic-enriched fractions (Kramer and Schulz-Schaeffer, 2007; Muntané *et al.*, 2008; Tanji *et al.*, 2010; Walker *et al.*, 2013). However, many of these studies could not specifically address the precise synaptic localization due to the low resolution of the techniques used. Our results confirm and expand on these observations in intact brain samples by using a technique especially suited for the analysis of human brain synapses.

We found that ~20% of p-α-synuclein aggregates were colocalizing with synaptophysin-positive terminals in the cingulate cortex and striatum. The percentage was a slightly higher (25%) when using synapsin I as a presynaptic marker. The detection of p-α-synuclein at pre-synaptic compartments suggests a role in synaptic degeneration. Notably, we found that small α-synuclein aggregates are the most common form in synapses. A previous study (Kramer and Schulz-Schaeffer, 2007) described proteinase-k-resistant aggregates in pre-synaptic compartments that represented the 50-90% of α-synuclein aggregates. We found a much lower percentage of α-synuclein aggregates at the pre-synaptic terminals. This difference may be due to numerous methodological differences: the antibodies used; the methods to detect synapses and pathological aggregates; or our stringent protocol used to define p-α-synuclein and ~~synaptophysin-containing~~presynaptic objects. Despite these methodological issues, we found that 77% of p-α-synuclein aggregates in contact with

pre-synaptic terminals are small aggregates. Taken together, both studies support the notion of small α-synuclein aggregates as key pathological forms in driving synaptic damage and dysfunction (Schulz-Schaeffer, 2010).

Our results are also in line with the hypothesis that the pre-synaptic terminal is an early site of α-synuclein aggregation in DLB and other α-synucleinopathies, the same site where it is found under physiological conditions (Lashuel *et al.*, 2013; Spinelli *et al.*, 2014; Volpicelli-Daley *et al.*, 2014; Majd *et al.*, 2015; Abeliovich and Gitler, 2016). The aggregation of α-synuclein may lead to abnormal functional impairment of neurotransmitter release (Garcia-Reitböck *et al.*, 2010; Nemani *et al.*, 2010), subsequent to axonal transport defects through the impairment of endosome and/or autophagosome transport (Volpicelli-Daley *et al.*, 2014), which may lead to neurodegeneration (Ferrer *et al.*, 2001; Desplats *et al.*, 2009; Decressac *et al.*, 2013).

We also observed larger pre-synaptic terminal volume in the presence of p-α-synuclein. Interestingly, an inverse correlation has been observed between synaptic density and the size of remaining synapses in Alzheimer's disease~~D~~ as measured by the length of the post-synaptic density (DeKosky and Scheff, 1990; Scheff *et al.*, 1990; Scheff and Price, 1993). This enlargement of remaining synapses has been interpreted as a compensatory response, rather than as selective loss of small synapses. Our data could suggest a similar compensatory mechanism in synapses containing pathological p-α-synuclein.

Several previous studies in cellular and animal models have shown that α-synuclein may propagate along neural circuits following a hierarchical pattern (Eisbach and Outeiro, 2013; Masuda-Suzukake *et al.*, 2013; Recasens and Dehay, 2014). The observation of a spatial gradient in p-α-synuclein aggregation in synapses (pre>pre+post>post-synaptic) could be interpreted as a sign of trans-synaptic spreading

of α-synuclein pathology. However, using Stimulated Emission Depletion microscopy we found that although p-α-synuclein predominates at the pre-synapse it can also be found independently at the post-synapse. Due to the inherent descriptive nature of post-mortem studies and the difficulties to identify the synaptic cleft, additional research is needed to elucidate if our findings are related to α-synuclein spreading and/or independent aggregation in both synaptic compartments. ~~another possible explanation for this observation may be the limited resolution of the technique to clearly dissociate the pre- and post-synapse.~~

Despite the limitations of our study ~~–~~relatively small sample size, ~~analysis of a single brain region~~inclusion of cases with advanced disease stages, or analysis of a single phospho-epitope of p-α-synuclein-, our findings are important as they demonstrate for the first time that p-α-synuclein accumulates in pre-synaptic terminals by large-scale imaging of synapses in DLB brain. Taken together, the present work provides a visual and quantitative evidence of the synaptic deposition of small p-α-synuclein aggregates in pre-synaptic terminals. This study supports the hypothesis that DLB and other α-synucleinopathies are primary synaptopathies. These data should stimulate the search for therapies aimed at reducing synaptic α-synuclein-induced damage or spread.

Acknowledgments

The authors would like to thank all brain donors and their relatives for generous brain donation for research. This research has been supported by Fundació Cellex Barcelona

Funding

This work was supported by FISPI14/1561, Fondo Europeo de Desarrollo Regional (FEDER), Unión Europea, "Una manera de hacer Europa",~~to A.L.,~~ PERIS SLT002/16/00408-01 and Marató TV3 to ~~A.L~~Alberto Lleó and CIBERNED. Colin Smith and Chris-Anne McKenzie were funded by MRC grant MR/L016400/1. Chris Henstridge is funded by a project grant from MND Scotland. The Massachusetts Alzheimer Disease Research Center is supported by funding from the NIH (P50 AG005134). Tara Spires-Jones is funded by the European Research Council (Consolidator award ALZSYN), Alzheimer's Research UK, the Scottish Government Chief Scientists' Office, Alzheimer's Society, and Wellcome Trust/University of Edinburgh Institutional Strategic Support Funding. Pablo Loza-Alvarez is funded by The Spanish Ministry of Economy and Competitiveness, through the "Severo Ochoa" Programme for Centres of Excellence in R&D (SEV- 2015-0522) and the CERCA Programme/Generalitat de Catalunya.

Conflict of interest

The authors report no potential conflict of interest. Tara Spires-Jones collaborates with Cognition Therapeutics but this collaboration is not relevant to this study.

References

Abeliovich A, Gitler AD. Defects in trafficking bridge Parkinson's disease pathology

and genetics. Nature 2016; 539: 207–216.

Anderson JP, Walker DE, Goldstein JM, De Laat R, Banducci K, Caccavello RJ, et al. Phosphorylation of Ser-129 is the dominant pathological modification of α-synuclein in familial and sporadic lewy body disease. J. Biol. Chem. 2006; 281: 29739–29752.

Bereczki E, Francis PT, Howlett D, Pereira JB, Höglund K, Bogstedt A, et al. Synaptic proteins predict cognitive decline in Alzheimer's disease and Lewy body dementia. Alzheimer's Dement. 2016; 12: 1–10.

Braak H, Del Tredici K, Rüb U, De Vos RAI, Jansen Steur ENH, Braak E. Staging of brain pathology related to sporadic Parkinson's disease. Neurobiol. Aging 2003; 24: 197–211.

Brown DF, Risser RC, Bigio EH, Tripp P, Stiegler a, Welch E, et al. Neocortical synapse density and Braak stage in the Lewy body variant of Alzheimer disease: a comparison with classic Alzheimer disease and normal aging. J. Neuropathol. Exp. Neurol. 1998; 57: 955–60.

Burré J. The synaptic function of alpha-synuclein. J. Parkinsons. Dis. 2015; 5: 699–713.

Calo L, Wegrzynowicz M, Santivañez-Perez J, Grazia Spillantini M. Synaptic failure and α-synuclein. Mov. Disord. 2016; 31: 169–177.

Campbell BC, Li QX, Culvenor JG, Jäkälä P, Cappai R, Beyreuther K, et al. Accumulation of insoluble alpha-synuclein in dementia with Lewy bodies. Neurobiol. Dis. 2000; 7: 192–200.

Chung CY, Koprich JB, Siddiqi H, Isacson O. Dynamic changes in presynaptic and axonal transport proteins combined with striatal neuroinflammation precede dopaminergic neuronal loss in a rat model of AAV alpha-synucleinopathy. J. Neurosci. 2009; 29: 3365–3373.

Clayton DF, George JM. Synucleins in synaptic plasticity and neurodegenerative disorders. J. Neurosci. Res. 1999; 58: 120–129.

Colom-Cadena M, Gelpi E, Charif S, Belbin O, Blesa R, Marti MJ, et al. Confluence of alpha-synuclein, tau, and beta-amyloid pathologies in dementia with Lewy bodies. J. Neuropathol. Exp. Neurol. 2013; 72: 1203–1212.

Decressac M, Mattsson B, Weikop P, Lundblad M, Jakobsson J, Björklund A. TFEB-mediated autophagy rescues midbrain dopamine neurons from α-synuclein toxicity. Proc. Natl. Acad. Sci. U. S. A. 2013; 110: E1817-26.

DeKosky ST, Scheff SW. Synapse loss in frontal cortex biopsies in Alzheimer's disease: Correlation with cognitive severity. Ann. Neurol. 1990; 27: 457–464.

Desplats P, Lee H-J, Bae E-J, Patrick C, Rockenstein E, Crews L, et al. Inclusion formation and neuronal cell death through neuron-to-neuron transmission of alpha-synuclein. Proc. Natl. Acad. Sci. U. S. A. 2009; 106: 13010–5.

Eisbach SE, Outeiro TF. Alpha-Synuclein and intracellular trafficking: Impact on the spreading of Parkinson's disease pathology. J. Mol. Med. 2013; 91: 693–703.

Ferrer I, Blanco R, Carmona M, Puig B, Barrachina M, Gómez C, et al. Active, phosphorylation-dependent mitogen-activated protein kinase (MAPK/ERK), stress-activated protein kinase/c-Jun N-terminal kinase (SAPK/JNK), and p38 kinase expression in Parkinson's disease and Dementia with Lewy bodies. J. Neural Transm. 2001; 108: 1383–1396.

Fujiwara H, Hasegawa M, Dohmae N, Kawashima A, Masliah E, Goldberg MS, et al. α-Synuclein is phosphorylated in synucleinopathy lesions. Nat. Cell Biol. 2002; 4: 160–164.

Garcia-Reitböck P, Anichtchik O, Bellucci A, Iovino M, Ballini C, Fineberg E, et al.

SNARE protein redistribution and synaptic failure in a transgenic mouse model of Parkinson's disease. Brain 2010; 133: 2032–2044.

Goedert M, Spillantini MG, Del Tredici K, Braak H. 100 years of Lewy pathology. Nat Rev Neurol 2013; 9: 13–24.

Hansen LA, Daniel SE, Wilcock GK, Love S. Frontal cortical synaptophysin in Lewy body diseases: relation to Alzheimer's disease and dementia. J Neurol Neurosurg Psychiatry 1998; 64: 653–656.

Hasegawa M, Fujiwara H, Nonaka T, Wakabayashi K, Takahashi H, Lee VMY, et al. Phosphorylated alpha-synuclein is ubiquitinated in alpha-synucleinopathy lesions. J. Biol. Chem. 2002; 277: 49071–49076.

Henstridge CM, Pickett E, Spires-Jones TL. Synaptic pathology: A shared mechanism in neurological disease. Ageing Res. Rev. 2016; 28: 72–84.

Iwai A, Masliah E, Yoshimoto M, Ge N, Flanagan L, Rohan de Silva HA, et al. The precursor protein of non-Abeta component of Alzheimer's disease amyloid is a presynaptic protein of the central nervous system. Neuron 1995; 14: 467–475.

Jackson RJ, Rudinskiy N, Herrmann AG, Croft S, Kim JM, Petrova V, et al. Human tau increases amyloid β plaque size but not amyloid β-mediated synapse loss in a novel mouse model of Alzheimer's disease. Eur. J. Neurosci. 2016; 44: 3056–3066.

Kay KR, Smith C, Wright AK, Serrano-Pozo A, Pooler AM, Koffie R, et al. Studying synapses in human brain with array tomography and electron microscopy. Nat. Protoc. 2013; 8: 1366–80.

Khundakar AAA, Hanson PS, Erskine D, Lax NZ, Roscamp J, Karyka E, et al. Analysis of primary visual cortex in dementia with Lewy bodies indicates GABAergic involvement associated with recurrent complex visual hallucinations. Acta Neuropathol.

Commun. 2016; 4: 66.

Koffie RM, Hashimoto T, Tai HC, Kay KR, Serrano-Pozo A, Joyner D, et al. Apolipoprotein E4 effects in Alzheimer's disease are mediated by synaptotoxic oligomeric amyloid-beta. Brain 2012; 135: 2155–2168.

Koffie RM, Meyer-Luehmann M, Hashimoto T, Adams KW, Mielke ML, Garcia-Alloza M, et al. Oligomeric amyloid beta associates with postsynaptic densities and correlates with excitatory synapse loss near senile plaques. Proc. Natl. Acad. Sci. U. S. A. 2009; 106: 4012–7.

Kramer ML, Schulz-Schaeffer WJ. Presynaptic alpha-synuclein aggregates, not Lewy bodies, cause neurodegeneration in dementia with Lewy bodies. J. Neurosci. 2007; 27: 1405–1410.

Lashuel HA, Overk CR, Oueslati A, Masliah E. The many faces of α-synuclein: from structure and toxicity to therapeutic target. Nat. Rev. Neurosci. 2013; 14: 38–48.

Lundblad M, Decressac M, Mattsson B, Björklund A. Impaired neurotransmission caused by overexpression of α-synuclein in nigral dopamine neurons. Proc. Natl. Acad. Sci. U. S. A. 2012; 109: 3213–9.

Majd S, Power JH, Grantham HJM. Neuronal response in Alzheimer's and Parkinson's disease: the effect of toxic proteins on intracellular pathways. BMC Neurosci. 2015; 16: 69.

Maroteaux L, Campanelli JT, Scheller RH. Synuclein: a neuron-specific protein localized to the nucleus and presynaptic nerve terminal. J. Neurosci. 1988; 8: 2804–2815.

Masliah E, Mallory M, DeTeresa R, Alford M, Hansen L. Differing patterns of aberrant neuronal sprouting in Alzheimer's disease with and without Lewy bodies. Brain Res.

1993; 617: 258–266.

Masuda-Suzukake M, Nonaka T, Hosokawa M, Oikawa T, Arai T, Akiyama H, et al. Prion-like spreading of pathological alpha-synuclein in brain. Brain 2013; 136: 1128–1138.

McKeith IG, Dickson DW, Lowe J, Emre M, O'Brien JT, Feldman H, et al. Diagnosis and management of dementia with Lewy bodies: Third report of the DLB consortium. Neurology 2005; 65: 1863–1872.

Merino D, Mallabiabarrena A, Andilla J, Artigas D, Zimmermann T, Loza-Alvarez P. STED imaging performance estimation by means of Fourier transform analysis. Biomed. Opt. Express 2017; 8: 2472–2482.

Micheva KD, Smith SJ. Array Tomography: A New Tool for Imaging the Molecular Architecture and Ultrastructure of Neural Circuits. Neuron 2007; 55: 25–36.

Montine TJ, Phelps CH, Beach TG, Bigio EH, Cairns NJ, Dickson DW, et al. National institute on aging-Alzheimer's association guidelines for the neuropathologic assessment of Alzheimer's disease: A practical approach. Acta Neuropathol. 2012; 123: 1–11.

Mukaetova-Ladinska EB, Andras A, Milne J, Abdel-All Z, Borr I, Jaros E, et al. Synaptic proteins and choline acetyltransferase loss in visual cortex in dementia with Lewy bodies. J. Neuropathol. Exp. Neurol. 2013; 72: 53–60.

Muntané G, Dalfó E, Martinez A, Ferrer I. Phosphorylation of tau and α-synuclein in synaptic-enriched fractions of the frontal cortex in Alzheimer's disease, and in Parkinson's disease and related α-synucleinopathies. Neuroscience 2008; 152: 913–923.

Muntané G, Ferrer I, Martinez-Vicente M. A-Synuclein Phosphorylation and Truncation Are Normal Events in the Adult Human Brain. Neuroscience 2012; 200:

106–119.

Nemani VM, Lu W, Berge V, Nakamura K, Onoa B, Lee MK, et al. Increased Expression of α-Synuclein Reduces Neurotransmitter Release by Inhibiting Synaptic Vesicle Reclustering after Endocytosis. Neuron 2010; 65: 66–79.

Nikolaus S, Antke C, Müller HW. In vivo imaging of synaptic function in the central nervous system: II. Mental and affective disorders. Behav. Brain Res. 2009; 204: 32–66.

O'Rourke NA, Weiler NC, Micheva KD, Smith SJ. Deep molecular diversity of mammalian synapses: why it matters and how to measure it. Nat. Rev. Neurosci. 2012; 13: 365–79.

Recasens A, Dehay B. Alpha-synuclein spreading in Parkinson's disease. Front. Neuroanat. 2014; 8: 159.

Reid RT, Sabbagh MN, CoreyBloom J, Tiraboschi P, Thal LJ. Nicotinic receptor losses in dementia with Lewy bodies: Comparisons with Alzheimer's disease. Neurobiol. Aging 2000; 21: 741–746.

Revuelta GJ, Rosso A, Lippa CF. Neuritic pathology as a correlate of synaptic loss in dementia with lewy bodies. Am. J. Alzheimers. Dis. Other Demen. 2008; 23: 97–102.

Saito Y, Kawashima A, Ruberu NN, Fujiwara H, Koyama S, Sawabe M, et al. Accumulation of phosphorylated a-synuclein in aging human brain. J. Neuropathol. Exp. Neurol. 2003; 62: 644–654.

Samarasekera N, Salman RAS, Huitinga I, Klioueva N, McLean CA, Kretzschmar H, et al. Brain banking for neurological disorders. Lancet Neurol. 2013; 12: 1096–1105.

Scheff SW, DeKosky ST, Price DA. Quantitative assessment of cortical synaptic density in Alzheimer's disease. Neurobiol. Aging 1990; 11: 29–37.

Scheff SW, Price DA. Synapse loss in the temporal lobe in Alzheimer's disease. Ann. Neurol. 1993; 33: 190–199.

Schulz-Schaeffer WJ. The synaptic pathology of α-synuclein aggregation in dementia with Lewy bodies, Parkinson's disease and Parkinson's disease dementia. Acta Neuropathol. 2010; 120: 131–143.

Scott DA, Tabarean I, Tang Y, Cartier A, Masliah E, Roy S. A Pathologic Cascade Leading to Synaptic Dysfunction in alpha-Synuclein-Induced Neurodegeneration. Neurobiol. Dis. 2010; 30: 8083–8095.

Spinelli KJ, Taylor JK, Osterberg VR, Churchill MJ, Pollock E, Moore C, et al. Presynaptic alpha-synuclein aggregation in a mouse model of Parkinson's disease. J. Neurosci. 2014; 34: 2037–50.

Tanji K, Mori F, Mimura J, Itoh K, Kakita A, Takahashi H, et al. Proteinase K-resistant alpha-synuclein is deposited in presynapses in human Lewy body disease and A53T alpha-synuclein transgenic mice. Acta Neuropathol. 2010; 120: 145–154.

Thévenaz P, Ruttimann UE, Unser M. A pyramid approach to subpixel registration based on intensity. IEEE Trans. Image Process. 1998; 7: 27–41.

Vallortigara J, Rangarajan S, Whitfield D, Alghamdi A, Howlett D, Hortobágyi T, et al. Dynamin1 concentration in the prefrontal cortex is associated with cognitive impairment in Lewy body dementia. F1000Research 2014; 3: 108.

Volpicelli-Daley LA, Gamble KL, Schultheiss CE, Riddle DM, West AB, Lee VM-Y. Formation of α-synuclein Lewy neurite-like aggregates in axons impedes the transport of distinct endosomes. Mol. Biol. Cell 2014; 25: 4010–23.

Wakabayashi K, Honer WG, Masliah E. Synapse alterations in the hippocampal-entorhinal formation in Alzheimer's disease with and without Lewy body disease. Brain

Res. 1994; 667: 24–32.

Walker DG, Lue LF, Adler CH, Shill HA, Caviness JN, Sabbagh MN, et al. Changes in properties of serine 129 phosphorylated α-synuclein with progression of Lewy-type histopathology in human brains. Exp. Neurol. 2013; 240: 190–204.

Walker Z, Possin KL, Boeve BF, Aarsland D. Lewy body dementias. Lancet 2015; 386: 1683–1697.

Whitfield DR, Vallortigara J, Alghamdi A, Howlett D, Hortobágyi T, Johnson M, et al. Assessment of ZnT3 and PSD95 protein levels in Lewy body dementias and Alzheimer's disease: Association with cognitive impairment. Neurobiol. Aging 2014; 35: 2836–2844.

Xing H, Lim Y-A, Chong JR, Lee JH, Aarsland D, Ballard CG, et al. Increased phosphorylation of collapsin response mediator protein-2 at Thr514 correlates with β-amyloid burden and synaptic deficits in Lewy body dementias. Mol. Brain 2016; 9: 84.

Figure legends

Figure 1. Study design.

Tissue collection and processing of each case is shown in **A**. For each case, two adjacent tissue sections of cingulate cortex or the striatum (putamen nucleus) were processed and embedded in LR white. For each block a ribbon of >40 consecutive sections of 70nm was produced. Each ribbon was immunostained for synaptophysin (red), p-α-synuclein (green) and PSD-95 (cyan), synapsin I or α-synuclein, and nuclei were visualized with Hoescht 33258 (blue). Three subregions ~~of cortex~~ were imaged through the entire ribbon. In **B and C**, the processing and analysis of the images is summarized. **1.** First, individual channel stacks were produced, with all consecutive sections imaged. Consecutive sections of a reference channel (i.e. synaptophysin) were registered using a rigid and an affine transformation. Transformation matrices were applied to other channels. **2.** Second, images were segmented using an in-house algorithm based on local mean threshold segmentation, removing single section objects, filtering by size, and detecting three dimensional~~3D~~ objects as 6 neighbour connected components. Raw images (right) and segmented (left) representative images are shown. Each image corresponds to a single 70nm section with its corresponding orthogonal views. **3.** Neuropil area was calculated based on a maximum intensity projection of synaptophysin channel. **4.** Co-localization between the channels of interest and the sizes of co-localizing objects was calculated **5.** The object density and object size were quantified and **6.** For entire synaptic studies, segmented images of synaptophysin (pre-synaptic) and PSD-95 (post-synaptic) channels combined to remove all those objects without pre- and post-synaptic pairs. Abbreviations: Max Int, Maximum intensity; ~~-~~ 6n, six neighbour. Scale bar in A and B, 10µm; in C, 2µm.

Figure 2. P-α-synuclein immunoreactivity patterns and synaptic localization.

A Representative images of DLB, control and Alzheimer's disease cases stained with antibodies against synaptophysin (red) and p-α-synuclein (green). Each image is a maximum intensity projection of 31 consecutive sections. **B** Representative three dimensional~~3D~~ representations of types of p-α-synuclein aggregates (green) found in DLB cases ~~(green)~~ and synaptophysin terminals (red). Lewy bodies did not co-localize with synaptophysin terminals, while Lewy neurites and small aggregates did (arrowheads). **C** The quantification of total p-α-synuclein objects revealed that pathology was found almost exclusively in DLB cases (**, $p<0.01$). **D** Synaptograms representing six 70nm consecutive sections (from left to right ~~and top to bottom~~) of the Lewy neurite (LN) or small aggregate (SA) pointed by the arrowheads in **B**. ~~Are represented b~~Both the raw and segmented images are shown. ~~At right, t~~The percentage s of pre-synaptic p-α-synuclein found of LN or SA ~~that are pre-synaptic and the percentage of~~and extra-synaptic p-α-synuclein are indicated. Abbreviations: DLB, dementia with Lewy bodies; AD, Alzheimer disease; LN, Lewy neurite; SA, Small aggregate. Scale bar in A, 10µm; in B, 2µm; in D, 1µm.

Figure 3. Median volume of pre-synaptic terminals co-localizing with p-α-synuclein.

A Three dimensional reconstruction of 20 consecutive sections from a DLB case is shown. P-α-synuclein (green) and synaptophysin (red) are shown. Black arrowheads indicate synaptophysin objects that co-localize with small aggregates of p-α-synuclein, grey arrowheads point~~s~~ to synaptic terminals that co-localize with Lewy neurites, and white arrowheads those synaptophysin objects that do not co-localize with p-α-

synuclein. **B** Median volumes of synaptic terminals according to co-localization with p-α-synuclein (p-α-synuclein +, or -) and their characteristic pattern (small aggregate or Lewy neurite). Abbreviations: Psyn: Phosphorylated-α-synuclein; SA, small aggregate; LN, Lewy neurite. Scale bar in A, 2µm.

Figure 4. Trans-synaptic localization of p-α-synuclein.

A Three dimensional reconstruction of 20 consecutive sections from a DLB case. P-α-synuclein (green), synaptophysin (red) and PSD-95 (blue) are shown. White arrowheads point to zones where p-α-synuclein co-localizes with synaptophysin (pre-synaptic), PSD-95 (post-synaptic) or both (pre and post-synaptic). In **B**, p-α-synuclein objects that co-localized with synaptic pairs (synaptophysin and PSD-95 objects) are classified depending on its pre-synaptic, pre and post-synaptic or post-synaptic localization. The relative co-localization of p-α-synuclein with the synaptophysin pre-synaptic marker was significantly higher than the PSD-95 post-synaptic co-localization. **C** ~~A representative reconstruction of synaptic pairs from twenty 70 nm sections from a DLB case. Synaptophysin is shown in red and PSD-95 in cyan. The black square on the left image represents the inset magnified on the right image. At the bottom a synaptogram of ten 70nm consecutive sections is shown.~~ Representative images of the colocalization between between p-α-synuclein, synaptophysin and PSD-95 using –array tomography combined with Stimulated Emission Depletion microscopy. A single 70nm-thick section stained for p-α-synuclein (green), synaptophysin (red) and PSD-95 (blue) is shown. Stimulated Emission Depletion was applied to image PSD-95 (upper row) or p-α-synuclein (lower row). Abbreviations: STED, Stimulated Emission Depletion. Scale bar in A, 2µm; in C, 1µm.

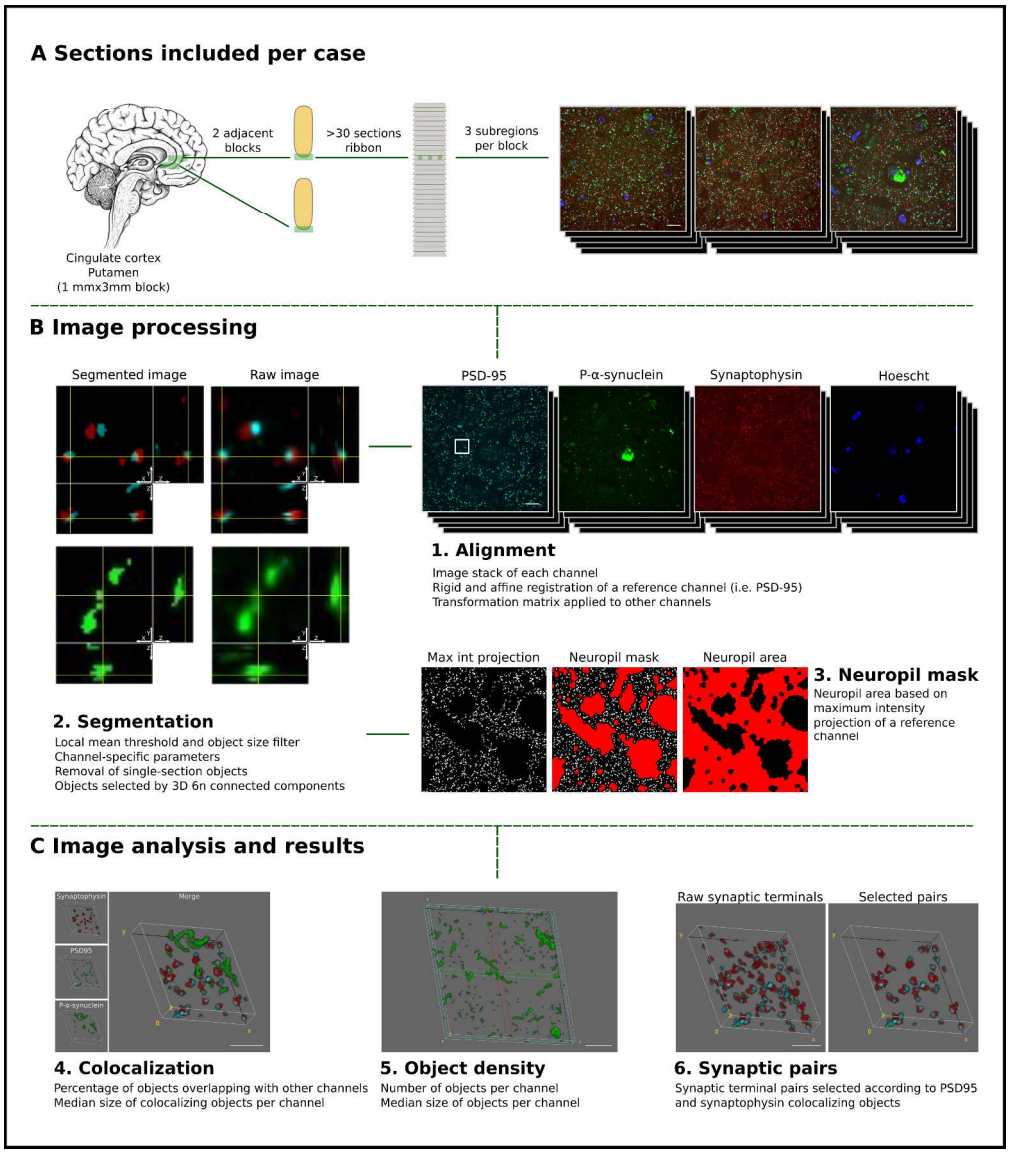

Figure 1. Study design.
Tissue collection and processing of each case is shown in A. For each case, two adjacent tissue sections of cingulate cortex or the striatum (putamen nucleus) were processed and embedded in LR white. For each block a ribbon of >40 consecutive sections of 70nm was produced. Each ribbon was immunostained for synaptophysin (red), p-α-synuclein (green) and PSD-95 (cyan), synapsin I or α-synuclein, and nuclei were visualized with Hoescht 33258 (blue). Three subregions were imaged through the entire ribbon. In B and C, the processing and analysis of the images is summarized. 1. First, individual channel stacks were produced, with all consecutive sections imaged. Consecutive sections of a reference channel (i.e. synaptophysin) were registered using a rigid and an affine transformation. Transformation matrices were applied to other channels. 2. Second, images were segmented using an in-house algorithm based on local mean threshold segmentation, removing single section objects, filtering by size, and detecting three dimensional objects as 6 neighbour connected components. Raw images (right) and segmented (left) representative images are shown. Each image corresponds to a single 70nm section with its corresponding orthogonal views. 3. Neuropil area was calculated based on a maximum intensity projection of synaptophysin channel. 4. Co-localization between the channels of interest and the sizes of co-localizing objects was calculated 5. The

object density and object size were quantified and 6. For entire synaptic studies, segmented images of synaptophysin (pre-synaptic) and PSD-95 (post-synaptic) channels combined to remove all those objects without pre- and post-synaptic pairs. Abbreviations: Max Int, Maximum intensity; 6n, six neighbour. Scale bar in A and B, 10μm; in C, 2μm.

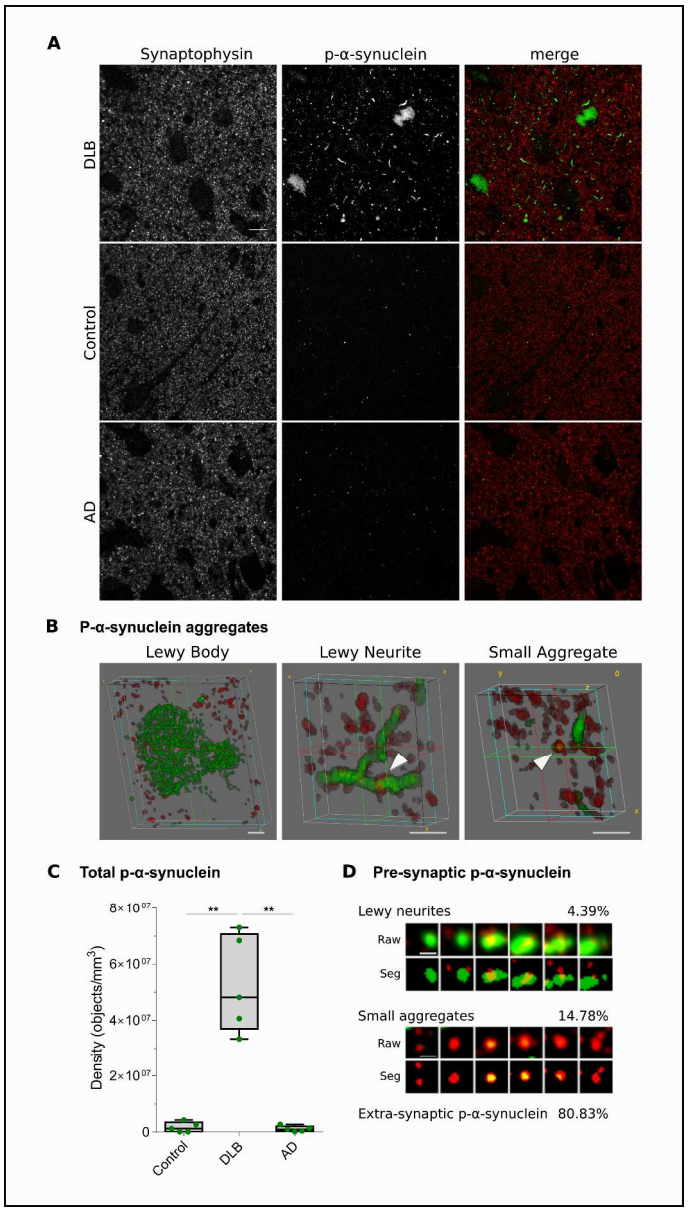

Figure 2. P-α-synuclein immunoreactivity patterns and synaptic localization.
A Representative images of DLB, control and Alzheimer's disease cases stained with antibodies against synaptophysin (red) and p-α-synuclein (green). Each image is a maximum intensity projection of 31 consecutive sections. B Representative three dimensional representations of types of p-α-synuclein aggregates (green) found in DLB cases and synaptophysin terminals (red). Lewy bodies did not co-localize with synaptophysin terminals, while Lewy neurites and small aggregates did (arrowheads). C The quantification of total p-α-synuclein objects revealed that pathology was found almost exclusively in DLB cases (**, $p<0.01$). D Synaptograms representing six 70nm consecutive sections (from left to right) of the Lewy neurite (LN) or small aggregate (SA) pointed by the arrowheads in B. Both the raw and segmented images are shown. The percentage s of pre-synaptic p-α-synuclein found of LN or SA and extra-synaptic p-α-synuclein are indicated. Abbreviations: DLB, dementia with Lewy bodies; AD, Alzheimer disease; LN, Lewy neurite; SA, Small aggregate. Scale bar in A, 10μm; in B, 2μm; in D, 1μm.

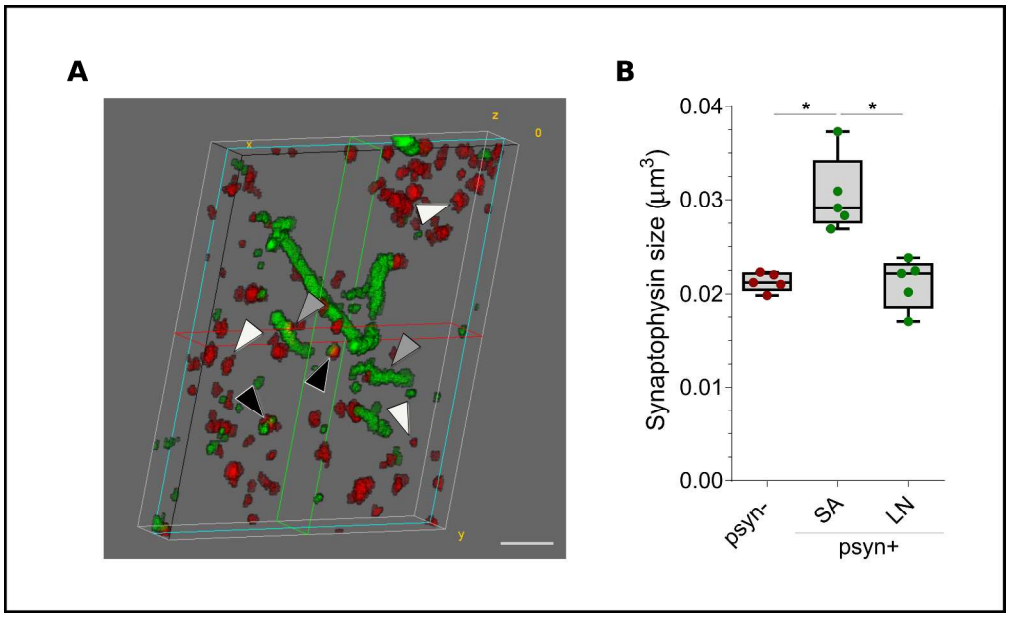

Figure 3. Median volume of pre-synaptic terminals co-localizing with p-α-synuclein.
A Three dimensional reconstruction of 20 consecutive sections from a DLB case is shown. P-α-synuclein (green) and synaptophysin (red) are shown. Black arrowheads indicate synaptophysin objects that co-localize with small aggregates of p-α-synuclein, grey arrowheads point to synaptic terminals that co-localize with Lewy neurites, and white arrowheads those synaptophysin objects that do not co-localize with p-α-synuclein. B Median volumes of synaptic terminals according to co-localization with p-α-synuclein (p-α-synuclein +, or -) and their characteristic pattern (small aggregate or Lewy neurite). Abbreviations: Psyn: Phosphorylated-α-synuclein; SA, small aggregate; LN, Lewy neurite. Scale bar in A, 2µm.

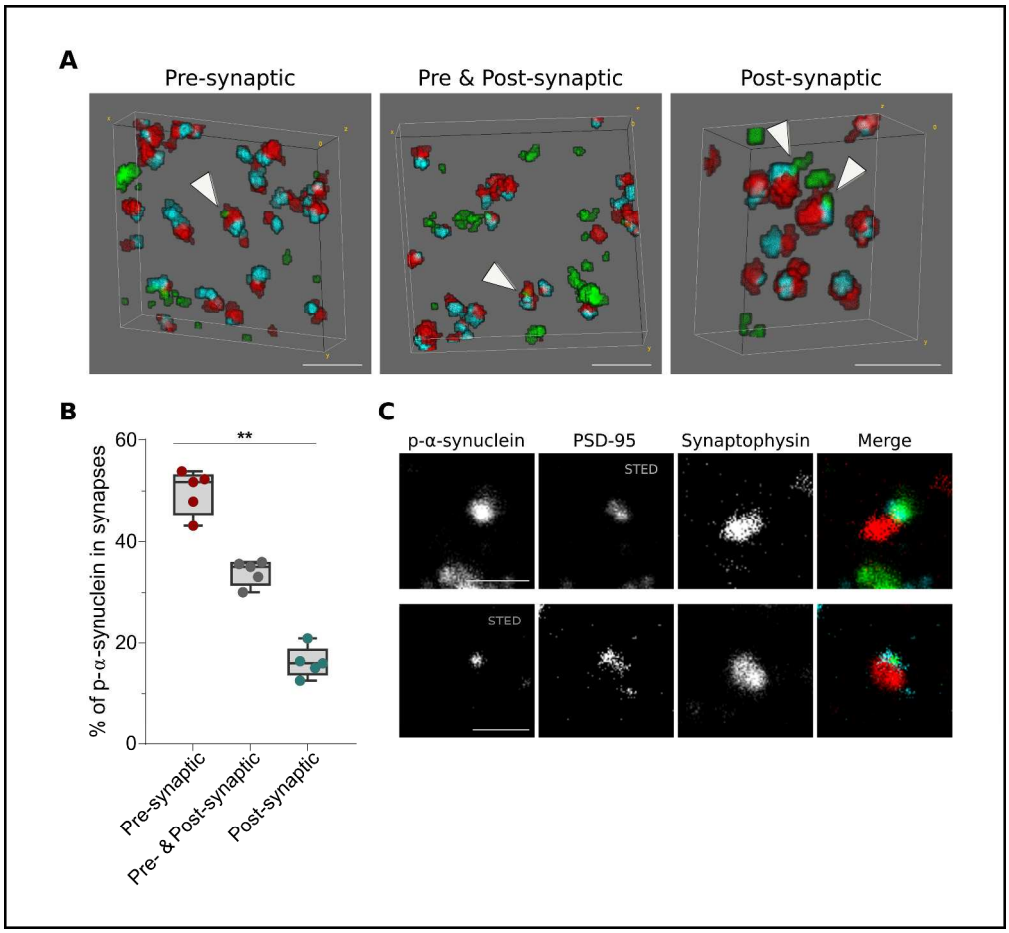

Figure 4. Trans-synaptic localization of p-α-synuclein.
A Three dimensional reconstruction of 20 consecutive sections from a DLB case. P-α-synuclein (green), synaptophysin (red) and PSD-95 (blue) are shown. White arrowheads point to zones where p-α-synuclein co-localizes with synaptophysin (pre-synaptic), PSD-95 (post-synaptic) or both (pre and post-synaptic). In B, p-α-synuclein objects that co-localized with synaptic pairs (synaptophysin and PSD-95 objects) are classified depending on its pre-synaptic, pre and post-synaptic or post-synaptic localization. The relative co-localization of p-α-synuclein with the synaptophysin pre-synaptic marker was significantly higher than the PSD-95 post-synaptic co-localization. C Representative images of the colocalization between between p-α-synuclein, synaptophysin and PSD-95 using array tomography combined with Stimulated Emission Depletion microscopy. A single 70nm-thick section stained for p-α-synuclein (green), synaptophysin (red) and PSD-95 (blue) is shown. Stimulated Emission Depletion was applied to image PSD-95 (upper row) or p-α-synuclein (lower row). Abbreviations: STED, Stimulated Emission Depletion. Scale bar in A, 2µm; in C, 1µm.

Table 1. Demographic, clinical and neuropathologic data of control, DLB and ~~AD~~ Alzheimer's disease cases.

Case	Diagnosis	Gender	Age at death	PMI (h)	McKeith type	LB Braak stage	Braak NFT stage
1	Control	M	82	24	-	0	0
2	Control	M	63	16	-	0	0
3	Control	F	77	75	-	0	I
4	Control	M	78	39	-	0	I
5	Control	F	83	8	-	0	II
6	DLB	M	71	8	Neocortical	5	III
7	DLB	M	83	24	Neocortical	5	IV
8	DLB	F	62	9	Neocortical	5	IV
9	DLB	M	77	36	Neocortical	5	III
10	DLB	F	83	24	Neocortical	6	VI
11	AD	M	81	74	-	0	V
12	AD	M	72	109	-	0	VI
13	AD	M	81	83	-	0	VI
14	AD	M	85	91	-	0	VI
15	AD	F	90	18	-	0	V

Abbreviations: PMI, Post-mortem interval; h, hours; LB, Lewy body; NFT, Neurofibrillary tangle; DLB, dementia with Lewy bodies; AD, Alzheimer disease.

Supplementary Data

Synaptic phosphorylated α-synuclein in dementia with Lewy bodies

Martí Colom-Cadena, Jordi Pegueroles, Abigail G. Herrmann, Christopher M. Henstridge, Laia Muñoz, Marta Querol-Vilaseca, Carla San Martin, Joan Luque-Cabecerans, Jordi Clarimon, Olivia Belbin, Raúl Núñez-Llaves, Rafael Blesa, Colin Smith, Chris-Anne McKenzie, Matthew P. Frosch, Allyson Roe, Juan Fortea, Jordi Andilla, Pablo Loza-Alvarez, Ellen Gelpi, Bradley T. Hyman, Tara L. Spires-Jones, Alberto Lleó

Supplementary Table 1. The Medical Research Council (MRC) Edinburgh Brain & Tissue Bank cases.

Case	BNN Number
SD063/13	19686
SD024/15	26495
SD056/14	24527
SD005/16	28410
SD010/16	28771

MRC numbers and associated BNN numbers.

Supplementary Figure 1. Distribution of non-phosphorylated and phosphorylated α-synuclein in dementia with Lewy bodies and controls.

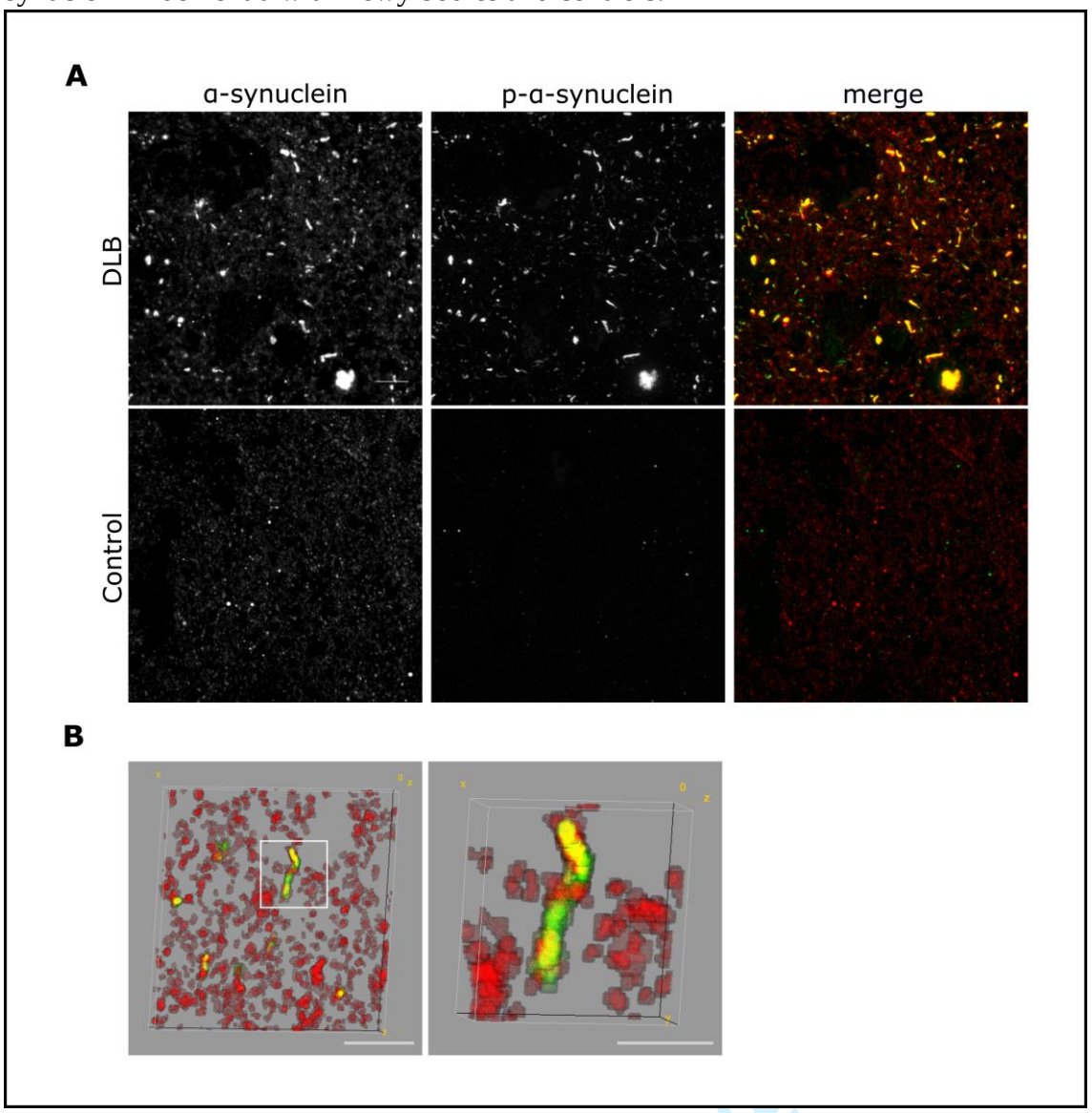

A Representative images of brain sections of a case with dementia with Lewy bodies and a control case stained with antibodies against non-phosphorylated α-synuclein (red) and p-α-synuclein (green). Each image is a maximum intensity projection of 20 consecutive sections. **B** Three dimensional representation of non-phosphorylated alpha-synuclein (red) and p-α-synuclein (green) aggregates found in DLB cases. An inset of the low magnification image is shown on the right. Abbreviations: DLB, dementia with Lewy bodies. Scale bar in A, 10µm; in B, 5µm (left) and 2µm (right).

Supplementary Figure 2. Segmentation and co-localization examples.

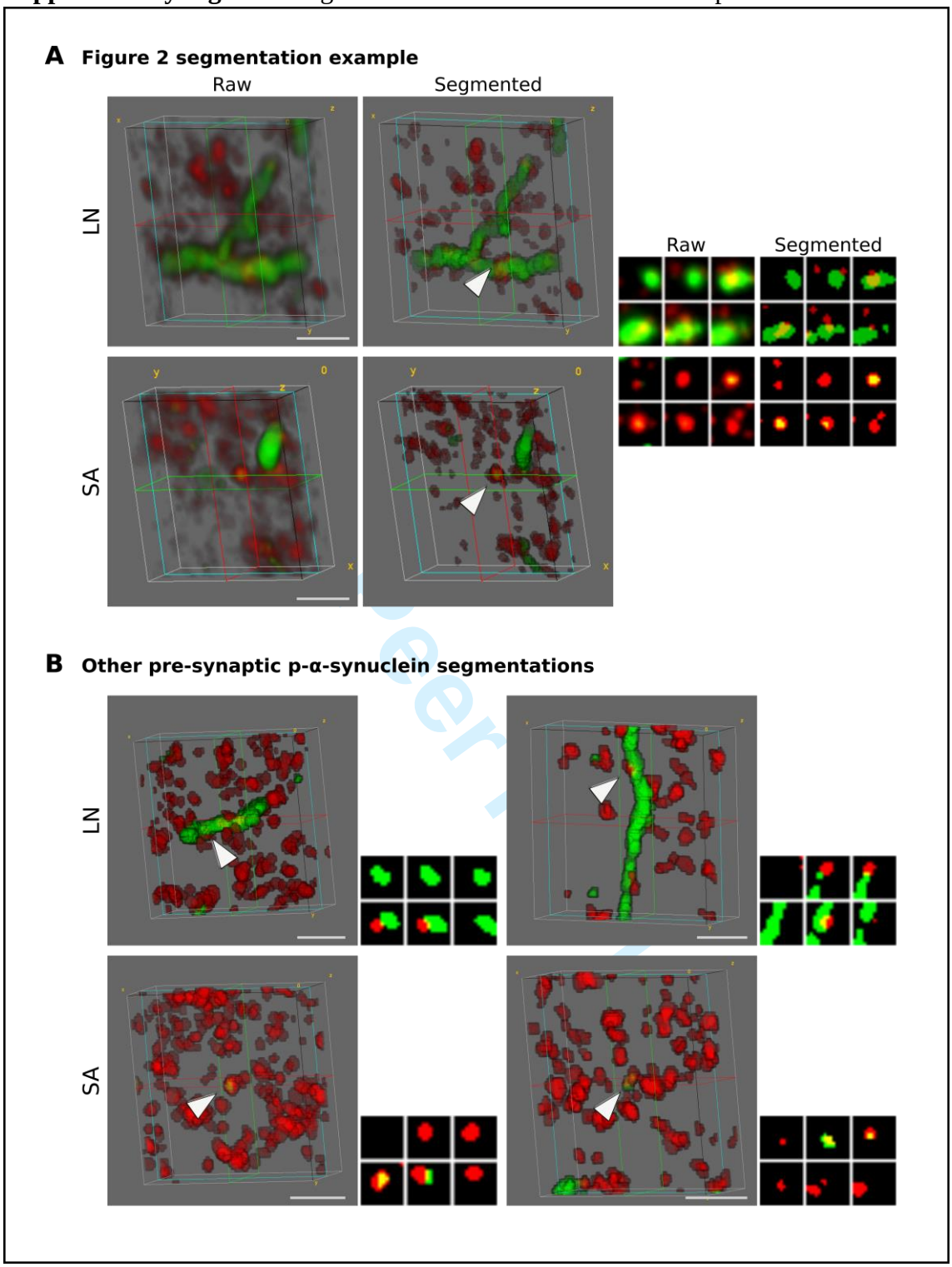

A Three dimensional representations of the images shown in Figure 2 as well as synaptograms representing six 70nm consecutive sections (from left to right and top to bottom) of a Lewy neurite (LN) or a small aggregate (SA) (green) colocalizing with synaptophysin (red) pointed by the arrowheads. Both the raw and segmented images are shown. **B** 3D examples of other segmented Lewy neurites and small aggregates. Synaptograms on the bottom-right represent a magnification of the pointed area. Abbreviations: LN, Lewy neurite; SA, Small aggregate. Scale bars in A and B, 2µm.

Supplementary Figure 3. Pre-synaptic localization of p-α-synuclein and synapsin I in DLB.

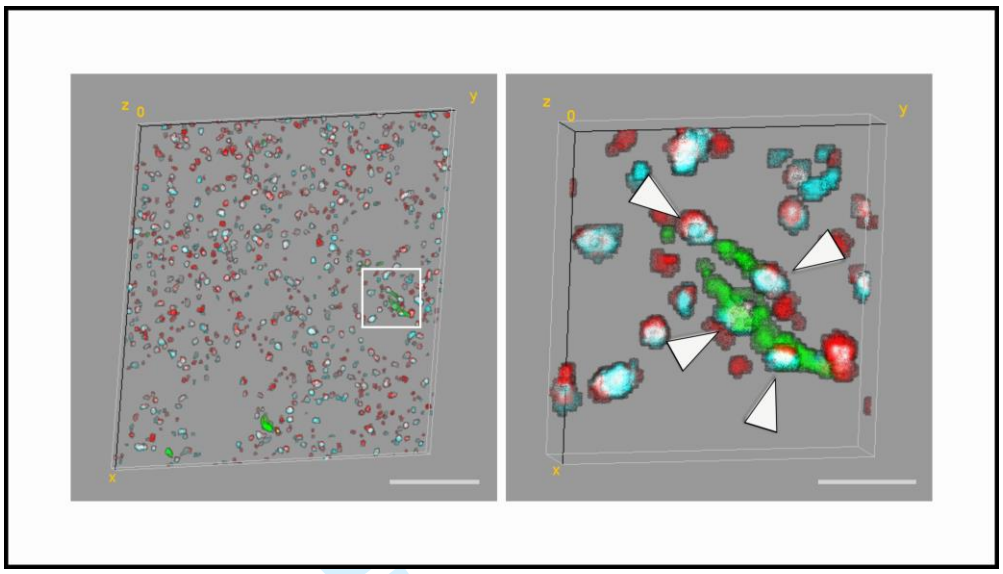

A Three dimensional reconstruction of 20 consecutive sections from a DLB case. P-α-synuclein (green), synaptophysin (red) and synapsin I (blue) are shown. An inset of the low magnification image is shown on the right. Arrowheads indicate objects with co-localization of all three markers. Scale bars 10µm (left) and 2µm (right).